Cerebellum (2012) 11:681–693
DOI 10.1007/s12311-010-0224-3

Controlling Ca^{2+}-Activated K^+ Channels with Models of Ca^{2+} Buffering in Purkinje Cells

Haroon Anwar · Sungho Hong · Erik De Schutter

Published online: 28 October 2010

Abstract Intracellular Ca^{2+} concentrations play a crucial role in the physiological interaction between Ca^{2+} channels and Ca^{2+}-activated K^+ channels. The commonly used model, a Ca^{2+} pool with a short relaxation time, fails to simulate interactions occurring at multiple time scales. On the other hand, detailed computational models including various Ca^{2+} buffers and pumps can result in large computational cost due to radial diffusion in large compartments, which may be undesirable when simulating morphologically detailed Purkinje cell models. We present a method using a compensating mechanism to replace radial diffusion and compared the dynamics of different Ca^{2+} buffering models during generation of a dendritic Ca^{2+} spike in a single compartment model of a PC dendritic segment with Ca^{2+} channels of P- and T-type and Ca^{2+}-activated K^+ channels of BK- and SK-type. The Ca^{2+} dynamics models used are (1) a single Ca^{2+} pool; (2) two Ca^{2+} pools, respectively, for the fast and slow transients; (3) detailed Ca^{2+} dynamics with buffers, pump, and diffusion; and (4) detailed Ca^{2+} dynamics with buffers, pump, and diffusion compensation. Our results show that detailed Ca^{2+} dynamics models have significantly better control over Ca^{2+}-activated K^+ channels and lead to physiologically more realistic simulations of Ca^{2+} spikes and bursting. Furthermore, the compensating mechanism largely eliminates the effect of removing diffusion from the model on Ca^{2+} dynamics over multiple time scales.

Keywords Purkinje cells · Calcium channels · Potassium channels · Calcium-activated · Calcium-binding proteins · Diffusion · Computer simulation

Introduction

Purkinje cells (PCs) are known to express large conductance (BK) [1–10] and small conductance (SK) [6, 11–14] Ca^{2+}-activated K^+ (K_{Ca}) channels on their dendrites. K_{Ca} channels together with voltage-gated Ca^{2+} channels significantly control the dendritic excitability [6, 15]. Ca^{2+} entering through the voltage-gated Ca^{2+} channels causes the free cytosolic Ca^{2+} concentration to rise, which in turn controls the activation of K_{Ca} channels. A significant difference between those channels is their spatial separation. It has been shown that BK channels are in closer vicinity of Ca^{2+} sources compared to SK channels, suggesting that BK channels require a brief large amount (~10–100 μM) of Ca^{2+}, while SK channels are activated by lower concentrations (~0–2 μM) [16–18]. Intracellular Ca^{2+} mechanisms like diffusion, endogenous buffers, internal stores, and pumps significantly control the cytosolic spread of Ca^{2+} and shape the Ca^{2+} signal that activates K_{Ca} channels [19]. Therefore, it is important to model intracellular Ca^{2+} dynamics carefully in a biophysically detailed PC model.

Existing PC models use a Ca^{2+} pool with a single relaxation time [20–22], which can reasonably approximate the fast transient [23] and can activate a BK channel well

Electronic supplementary material The online version of this article (doi:10.1007/s12311-010-0224-3) contains supplementary material, which is available to authorized users.

H. Anwar (✉) · S. Hong · E. De Schutter
Computational Neuroscience Unit,
Okinawa Institute of Science and Technology,
Okinawa 904-0411, Japan
e-mail: anwar@oist.jp

H. Anwar · E. De Schutter
Theoretical Neurobiology, University of Antwerp,
2610 Antwerp, Belgium

[17, 18]. On the other hand, it provides inappropriate Ca^{2+} signals to activate SK channels to support their role in excitability modulation. A simple and effective solution is to use two Ca^{2+} pools [24], respectively, for the fast and slow transient. A more comprehensive and biophysically realistic solution is to use a detailed model [25] with Ca^{2+} buffers, diffusion of those buffers, and diffusion of Ca^{2+} and Ca^{2+} extrusion pumps. Large compartments also require modeling of radial diffusion of Ca^{2+} ions and buffers [26]. The presence of diffusion in these detailed models can result in a large computational cost [27], which may need to be avoided in simulating morphologically detailed PC models.

In this study, we compare the effectiveness of different Ca^{2+} buffering models in controlling Ca^{2+}-activated K^+ channels. We build a single compartment model of a PC dendritic segment, including P-type and T-type voltage-gated Ca^{2+} channels and BK-type and SK-type Ca^{2+} -activated K^+ channels, and tune this to generate Ca^{2+} spikes. Intracellular Ca^{2+} dynamics are modeled using a single Ca^{2+} pool, two Ca^{2+} pools, or detailed Ca^{2+} dynamics with calbindin (CB), parvalbumin (PV), a pump, and diffusion. Our results show that a detailed Ca^{2+} dynamics model with buffers, pumps, and diffusion has better control over Ca^{2+}-activated K^+ channels and can generate physiologically more realistic Ca^{2+} spikes. We also introduce a method to specify a diffusion compensating mechanism (DCM) that can replace the radial diffusion in the model. Our result shows that the consequences of removing diffusion from the model on the simulated Ca^{2+} dynamics can be largely eliminated by these compensating mechanisms for both short and long time scales. This allows the generation of physiologically realistic Ca^{2+} spikes that can be simulated with significantly less computational cost.

Materials and Methods

PC Model for Ca^{2+} Spikes

A dendritic compartment with a diameter of 4 μm and a length of 20 μm was used as a PC dendrite model for simulating dendritic Ca^{2+} spikes. All the simulations were run in the NEURON simulation environment [28]. The details about the currents used in our model are given below.

P-Type Ca^{2+} Channel

The P-type calcium current was based on data from Swensen and Bean [29] and included three activation (m) gates. The current density was based on the Goldman–Hodgkin–Katz equation [30]. The equations describing its kinetics are summarized below:

$$I_{Ca^{2+}} = \overline{P_{Ca^{2+}}} \times m^3 \times g_{GHK}$$

$$m_\infty = \frac{1}{1+e^{-\frac{V+24.758}{8.429}}}$$

$$\tau_m = \left\{ \begin{array}{ll} 0.2702 + 1.1622e^{-\frac{(V+22.098)^2}{164.19}} & \text{if } V \geq -40\,\text{mV}, \\ 0.6923e^{\frac{V-4.7}{1{,}089.372}} & \text{otherwise} \end{array} \right\}$$

The factor g_{GHK} is a current per unit permeability.

T-Type Ca^{2+} Channel

The low threshold voltage-activated, T-type calcium current was modeled using Cav 3.1 data from Iftinca et al. [31]. It included two activation (m) gates and an inactivation (h) gate. The current density is based on the Goldman–Hodgkin–Katz equation [30]. The equations describing its kinetics are summarized below:

$$I_{Ca^{2+}} = \overline{P_{Ca^{2+}}} \times m^2 \times h \times g_{GHK}$$

$$m_\infty = \frac{1}{1+e^{-\frac{V+52}{5}}}, \quad \tau_m = \left\{ \begin{array}{ll} 1 & \text{if } V \leq -90\,\text{mV}, \\ 1 + \frac{1}{e^{\frac{V+40}{9}} + e^{-\frac{V+102}{18}}} & \text{otherwise} \end{array} \right\}$$

$$h_\infty = \frac{1}{1+e^{\frac{V+72}{7}}}, \quad \tau_h = 15 + \frac{1}{e^{\frac{V+32}{7}}}$$

The factor g_{GHK} is a current per unit permeability.

BK-Type K_{Ca} Channel

The BK-type K_{Ca} channel was based on a kinetic scheme proposed by Cox et al. [32]. The channel model has a single voltage-dependent gate and four binding sites for Ca^{2+} ions, and Ca^{2+} binding at each site modulates the opening/closing rate coefficients. The kinetic scheme and rate constants used in the BK model were obtained from scheme II and patch 3 data in Table III in reference [32].

SK-Type K_{Ca} Channel

We used the SK-type channel from a Golgi cell model [33], which was based on data from Hirschberg et al. [34].

Leak Current

The leak current was modeled as a linear voltage-independent conductance following Ohm's law:

$$I_{leak} = G_{leak}(V - E_{leak}),$$

where $G_{leak} = 10^{-6}\,\text{S/cm}^2$ and $E_{leak} = -61\,\text{mV}$.

Intracellular and Extracellular Ca^{2+}

Intracellular Ca^{2+} was modeled using different buffering mechanisms described in the following section. Extracellular Ca^{2+} was maintained at 2 mM during all the simulations.

Ca^{2+} Buffering Models

Intracellular Ca^{2+} was modeled using the following Ca^{2+} buffering mechanisms.

Single Pool

The exponential decaying Ca^{2+} pool was modeled as

$$\frac{d\left[Ca^{2+}{}_i\right]}{dt} = -\frac{I_{Ca^{2+}}(t)}{2Fd} - \beta\left(\left[Ca^{2+}{}_i\right] - \left[Ca^{2+}{}_o\right]\right),$$

where $\left[Ca^{2+}{}_i\right]$ is intracellular Ca^{2+}, $\left[Ca^{2+}{}_o\right]$ is Ca^{2+} at rest and is 45 nM, $I_{Ca^{2+}}(t)$ is total current through P-type and T-type Ca^{2+} channels, F is Faraday's constant, d is depth of a submembrane shell to define the volume for effective Ca^{2+} concentration, and β is the decay time constant. Instead of using commonly used values for β and d, we tuned these parameters to approximate the Ca^{2+} transients given by detailed Ca^{2+} dynamics, as described in the "Tuning of Single Pool Models" section.

Two Pools

Fast and slow Ca^{2+} transients, $\left[Ca^{2+}{}_i\right]_f$ and $\left[Ca^{2+}{}_i\right]_s$, were modeled using two pools with different decay time constants, β_f and β_s ($\beta_f > \beta_s$), and depths, d_f and d_s ($d_f < d_s$). The total intracellular Ca^{2+} $\left[Ca^{2+}{}_i\right]$ was modeled as the weighted sum of fast and slow Ca^{2+} transients.

$$\left[Ca^{2+}{}_i\right] = f_f\left[Ca^{2+}{}_i\right]_f + f_s\left[Ca^{2+}{}_i\right]_s$$

The parameters β_f, β_s, d_f, d_s, f_f, and f_s were tuned to approximate the Ca^{2+} transients given by detailed Ca^{2+} dynamics, as described in the "Tuning of Double Pool" section.

Detailed Ca^{2+} Dynamics

The detailed Ca^{2+} dynamics model included calbindin (CB) and parvalbumin (PV) as buffers. In addition to Ca^{2+}, both PV and 80% of CB were diffusible. A single surface-based Ca^{2+} pump was modeled using Michaelis–Menten kinetics [35]. The kinetics of CB and PV was obtained from a pre-existing Ca^{2+} dynamics model [25] and is described in Table 1. The kinetics of the pump was tuned to approximately match the Ca^{2+} decay measured at very high intracellular Ca^{2+} concentration [36], where the buffers are almost saturated and the decay is solely due to pump and diffusion. The outer radial shell had a depth (d) of 0.1 μm, whereas other radial shells had a depth of 0.2 μm each.

Detailed Ca^{2+} Dynamics with Diffusion Compensation

The detailed Ca^{2+} dynamics model was modified by removing the diffusion of Ca^{2+} and buffers. A diffusion compensating mechanism (DCM) was included to compensate for the reduced removal of Ca^{2+} from the submembrane region due to the lack of diffusion towards the center of the compartment. The DCM follows a standard buffering scheme:

$$\left[Ca^{2+}\right] + [\mathrm{DCM}] \underset{k_{off}}{\overset{k_{on}}{\rightleftharpoons}} \left[Ca^{2+} - \mathrm{DCM}\right]$$

The total concentration of DCM and rate constants (k_{on} and k_{off}) were tuned to compensate for the diffusion of Ca^{2+} and mobile buffers in the absence of radial diffusion. Moreover, the depth of the single submembrane shell, which was used to compute the effective Ca^{2+} concentration for K_{Ca} channels, was also a tunable parameter.

Tuning of Ca^{2+} Buffering Models

Generating Target Traces

A single compartment was modeled with a diameter of 4 μm and a length of 20 μm. The P-type channel was included in the model for Ca^{2+} influx, and the detailed Ca^{2+} dynamics were used as a buffering model. A voltage step protocol, shown in Fig. 1a, was used to depolarize the compartment to the voltage at which physiological dendritic Ca^{2+} spikes are generated (an example of an experimental recording is shown for comparison in Fig. 1b). Then, different conductance values for P-type Ca^{2+} channel were used to generate peak amplitude of Ca^{2+} concentrations of 0.5, 1, 2, 4, and 8 μM in the volume defined by the submembrane shell. These simulated calcium transients formed the target traces for the automated fitting.

Similarly, the experimental voltage trace of Ca^{2+} spikes, shown in Fig. 1b, was used as the voltage clamp control signal to generate calcium transients with peak amplitudes of Ca^{2+} concentrations of ~1.25, 2.5, 5, and 10 μM. These simulated calcium transients were later used to tune parameters for pool-based Ca^{2+} buffering models.

Tuning of Single Pool Models

The same model as described above was used, but now with a single pool. We used Neurofitter [37], an automated parameter search method to find optimal values of d and β to match the single pool simulations with the target traces. We used the random search mode, and model traces were compared to the target using a standard root mean square (RMS) error measure. While using the step voltage protocol (shown in Fig. 1a), since each of the traces used in fitting

Table 1 Detailed Ca^{2+} dynamics model parameters

Parameter	Value	Reference
$[Ca^{2+}]$ at rest	45 nM	[43]
$[Mg^{2+}]$ at rest	590 μM	[25]
Diffusion rates		
DCa	0.233 $\mu m^2/ms$	[44]
DCB	0.028 $\mu m^2/ms$	[25]
DPV	0.043 $\mu m^2/ms$	[25]
Calbindin		
Concentration	0.16 mM	–[a]
$k_{on,fast}$	43.5 ms^{-1} mM^{-1}	[45]
$k_{off,fast}$	3.58×10^{-2} ms^{-1}	[45]
$k_{on,slow}$	5.5 ms^{-1} mM^{-1}	[45]
$k_{off,slow}$	0.26×10^{-2} ms^{-1}	[45]
Parvalbumin		
Concentration	0.08 mM	–[a]
$k_{on,Ca}$	107 ms^{-1} mM^{-1}	[25]
$k_{off,Ca}$	9.5×10^{-4} ms^{-1}	[46]
$k_{on,Mg}$	0.8 ms^{-1} mM^{-1}	[25]
$k_{off,Mg}$	2.5×10^{-2} ms^{-1}	[46]
Pump		
Density	1×10^{-9} mol cm^{-2}	Estimated
k_{on}	3×10^{-3} ms^{-1} mM^{-1}	Estimated
k_{off}	1.75×10^{-5} ms^{-1}	Estimated
k_{ext}	7.255×10^{-5} ms^{-1} mM^{-1}	Estimated
Fraction of immobile calbindin	0.2	[25]

[a] Data provided by Dr. Klaus M. Stiefel, personal communication

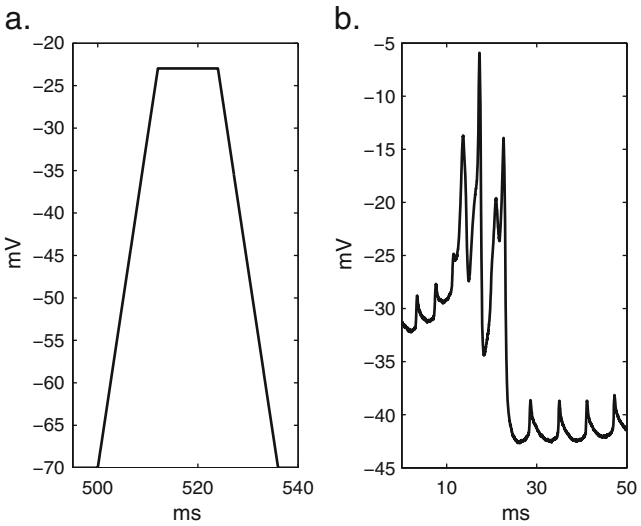

Fig. 1 **a** The depolarization command used to estimate Ca^{2+} profiles during generation of Ca^{2+} spikes. The peak voltage −22 mV was computed by taking an average of membrane potential during Ca^{2+} spikes (as shown in **b**), and the time of peak voltage ~12 ms was estimated from their average duration. **b** An example of electrophysiological dendritic Ca^{2+} spikes (provided by Ede Rancz and Michael Häusser, UCL, UK). Note that the small spikelets caused by retrograde conduction of somatic action potentials are not modeled in this study

had two distinct features: (1) a fast rise and decay and (2) a slow decay (Fig. 3), we separated those features by specifying two time periods, 500 to 550 ms and 550 to 5,000 ms, over which separate RMS values were computed and added together. Similarly, while using the experimental voltage protocol (shown in Fig. 1b), we separated each of the traces used in fitting by specifying two time periods, 10 to 25 ms and 25 to 50 ms, over which separate RMS values were computed and added together. The best values for d and β obtained to fit the data from Fig. 1b were used with the single pool model to simulate dendritic Ca^{2+} spikes.

Tuning of Double Pool

Similar procedures were used to search for the values of β_f, β_s, d_f, d_s, f_f, and f_s values.

Tuning of DCM

We replaced diffusion of Ca^{2+}, of free mobile buffers, and Ca^{2+}-bound mobile buffers (keeping the total buffer concentrations constant) from the detailed Ca^{2+} dynamics model with a single equation for DCM. Similar procedures were used as in the case of tuning the single pool, except

that we only used target traces generated using the step voltage protocol (shown in Fig. 1a), to find values of [DCM], k_{on}, k_{off}, and d. In order to find a robust solution, Neurofitter was run with five different seeds for random number generation. The five best solutions found using each seed were selected. We assume that the parameters for the diffusion compensating mechanism should be robust for different Ca^{2+} concentration peak amplitudes, but not for different compartment diameters. Therefore, the fitting procedure was repeated for diameters of 0.8, 2, 4, 6, 8, 10, 12, 16, and 20 μm.

DCM Parameter Interpolation

In actual compartmental models of neurons [38], a compartment can have an arbitrary diameter. Therefore, the parameters fitted to specific diameters were fitted to continuous functions. The 25 best solutions for each of the four parameters were plotted against corresponding diameter values. Matlab routines were used to fit the data with a single exponential function, double exponential function, and fifth order polynomial function based on an RMS measure. Later, those functions were used to predict the diffusion compensating parameter values for any compartment diameter.

Tuning Channel Densities for Dendritic Ca^{2+} Spikes

A dendritic Ca^{2+} spike, with three spikelets, was generated using the detailed Ca^{2+} dynamics model by hand tuning the channel density values. Later, Neurofitter was used to search proper channel densities for models with single pool, double pool, or DCM to generate similar dendritic Ca^{2+} spikes. The search was based on the RMS error measurement. We used five features for the fitness function. Three features comprised the three spikelets; other features were the pre-spike depolarization and post-spike hyperpolarization.

Results

Detailed Ca^{2+} Dynamics Model

A single compartment model with 4 μm diameter and 20 μm length was simulated with a P-type Ca^{2+} channel and the detailed Ca^{2+} dynamics model. The detailed Ca^{2+} dynamics model included calbindin (CB) and parvalbumin (PV) as buffers. The four binding sites of CB were simulated by assuming a pair of fast and a pair of slow binding sites as, respectively, a single fast and a single slow binding site (described as CB_f_s). PV was simulated together with Mg^{2+}. Due to medium affinity of PV for Mg^{2+}, its binding kinetics to Ca^{2+} is significantly affected by Mg^{2+}. Diffusion of Ca^{2+}, PV, and 80% of CB was included in the model. We simulated the voltage step of Fig. 1a in our model using different conductance values for P-type Ca^{2+} channel to generate peak amplitudes of 0.5 to 8 μM Ca^{2+} concentration. As the intracellular Ca^{2+} concentration started rising due to the influx through the P-type channel, the buffers and the pump became active. The changes in concentration of Ca^{2+} and Ca^{2+}-bound buffers and outflux due to the pump over time are shown in Fig. 2.

Dynamics of Single Pool and Double Pool Models

The pool parameters were tuned with Neurofitter [37], as described in "Materials and Methods" section. The best solution for the single pool, using the step voltage protocol (Fig. 1a), was β=1.35/ms and d= 0.891 μm. The best parameter values for the double pool were β_f=3.77/ms, d_f= 0.351 μm, β_s=0.00306/ms, d_s=0.928 μm, f_f=0.994, and f_s=0.006.

Figure 3 compares the intracellular Ca^{2+} profiles obtained using the tuned single pool and double pool models with those in the detailed Ca^{2+} dynamics model. The comparison demonstrates that the single pool approximates the Ca^{2+} transient only during the active Ca^{2+} influx and the initial fast decay. Moreover, the approximation is valid only for a small range of Ca^{2+} influx. Therefore, the single pool cannot approximate the effects of physiological buffering. The double pool can approximate Ca^{2+} transient during the active Ca^{2+} influx and following fast and slow Ca^{2+} decays, but its validity is also limited to a small range of Ca^{2+} influx values. Although the double pool model could not approximate the full range of detailed Ca^{2+} concentrations, it approximated the major components of the detailed model reasonably well, i.e., the fast and slow transients. Therefore, a double pool model is expected to provide a better control over activation of K_{Ca} channels than a single pool model.

Since these estimated parameters belong to phenomenological models, the parameter values could vary based on the applied protocol. To estimate the ability of pool-based models to capture more complex Ca^{2+} kinetics, we applied also the experimental waveform (Fig. 1b) and estimated new model parameters. The best solution for the single pool was very different from the model used in Fig. 3: β=6.86/ms and d= 0.169 μm. The same applied to the best parameter values for the double pool, though the ratio between fast and slow pool did not change: β_f=7.33/ms, d_f=0.167 μm, β_s=0.00795/ms, d_s=0.683 μm, f_f=0.995, and f_s=0.005. The behavior of these models (Supplementary Fig. 1) was similar to that observed in Fig. 3: their optimal concentration range is limited, and a single pool model cannot capture the slow transients.

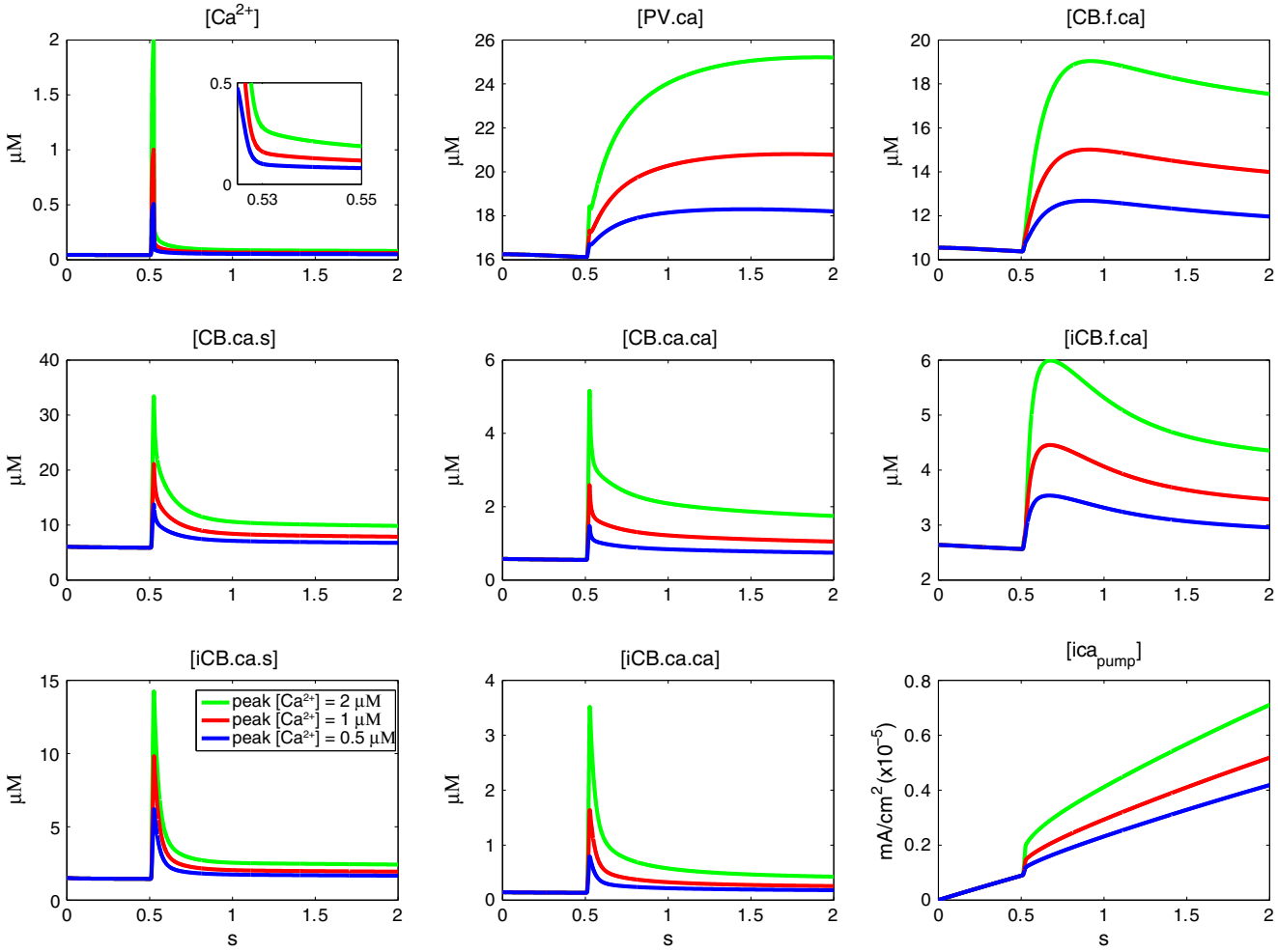

Fig. 2 Intracellular Ca^{2+} profiles simulated using the depolarization command shown in Fig. 1a, for different amplitudes of Ca^{2+} influx (indicated by *color*). The panels show, respectively, Ca^{2+} concentration ($[Ca^{2+}]$), Ca^{2+} bound to PV (PV.ca), Ca^{2+} bound to slow binding site of CB (CB.f.ca), Ca^{2+} bound to fast binding site of CB (CB.ca.s), Ca^{2+} bound to fast and slow binding sites (CB.ca.ca), Ca^{2+} bound to slow binding site of immobile CB (iCB.f.ca), Ca^{2+} bound to fast binding site of immobile CB (iCB.ca.s), Ca^{2+} bound to fast and slow binding sites (iCB.ca.ca), and pump current over a period of 2,000 ms

Diffusion Compensation Model

Modeling buffers and pumps without diffusion of Ca^{2+} and buffers resulted in an accumulation of Ca^{2+} in the submembrane volume defined by a shell of depth 0.1 µm in compartments with a diameter of 1 µm or larger (Fig. 4). Therefore, we developed a compensating mechanism, DCM, to reduce the steep rise in peak amplitudes of intracellular Ca^{2+}. Because the detailed Ca^{2+} dynamics model had multiple buffers with different buffer affinities, the effects of diffusion depended on the amount of Ca^{2+} entry. We developed DCM to robustly reproduce model Ca^{2+} transients in compartments with a wide range of diameters and for physiological peak amplitudes in the submembrane shell of between 0.5 and 8 µM.

The parameters for DCM were estimated using Neurofitter [37]. Examples for different levels of Ca^{2+} influx using the voltage step protocol demonstrate the effect of removing diffusion, and the good compensation by the DCM over the entire range is shown in Fig. 4.

Derivation of the Parameter Predictors

We showed in Fig. 4 that DCM can effectively compensate for excluding diffusion, but the parameter fitting produced values only for specific compartment diameters. To use DCM in a morphologically detailed PC model, we need a way to predict the DCM parameter values for any diameter present in the PC. Figure 5 shows the results of automated parameter fitting (see "Materials and Methods" section), for

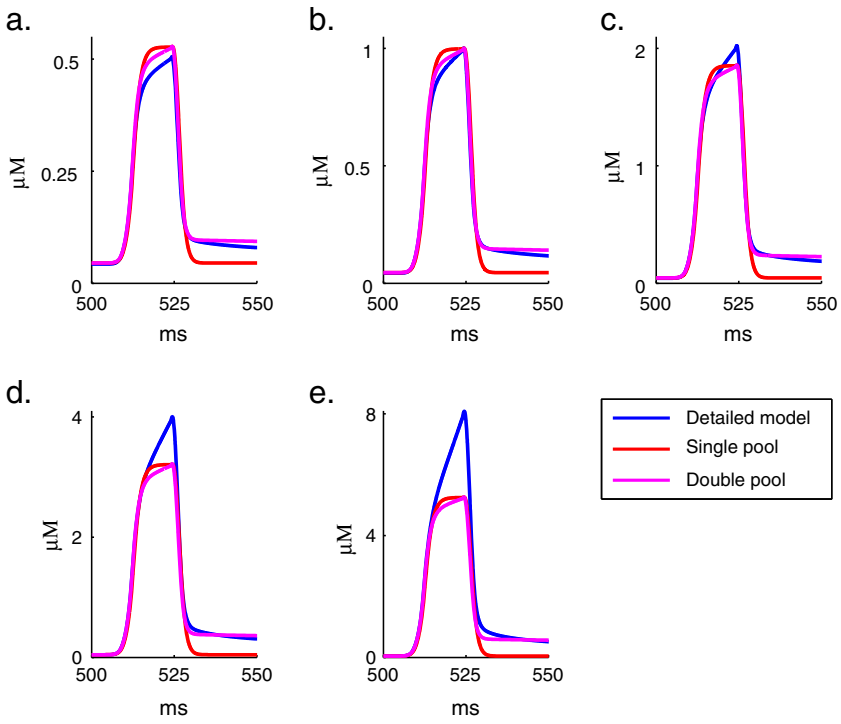

Fig. 3 Comparison of Ca^{2+} profiles generated with a voltage step protocol using single pool, double pool (parameters specified in the text), and detailed dynamics model. Different Ca^{2+} concentration peak amplitudes of **a** 0.5, **b** 1, **c** 2, **d** 4, and **e** 8 μM were simulated to demonstrate the problems the single pool or double pool models have in capturing the complex dynamics of the detailed model. See text for parameters of the pool models

nine diameters. Using Matlab, the four parameters (concentration of DCM, [DCM]; forward rate constant, k_{on}; the backward rate constant, k_{off}; and the depth of submembrane shell, d) were fitted to functions (Fig. 5). The prediction functions for the parameters are

$$[\mathrm{DCM}] = 64.2 - 57.3e^{-\frac{\mathrm{diam}}{1.4}}$$

$$k_{on} = 0.162 - 0.106e^{-\frac{\mathrm{diam}}{2.29}}$$

$$k_{off} = \begin{cases} 0.000267 + 0.0167e^{-\frac{\mathrm{diam}}{0.722}} + 0.0028e^{-\frac{\mathrm{diam}}{4}} & \text{if diam} \geq 2, \\ 0.003 & \text{otherwise} \end{cases}$$

$$d = \frac{\mathrm{diam}}{4\times\left(-0.674+1.94(\mathrm{diam})+0.289(\mathrm{diam})^2-3.33\times10^{-2}(\mathrm{diam})^3+1.55\times10^{-3}(\mathrm{diam})^4-2.55\times10^{-5}(\mathrm{diam})^5\right)}$$

The fitted functions are very close to the mean values of the parameter distributions and reasonably capture the relationship between the DCM parameters and the diameter of the compartment. Therefore, we expect these functions to predict DCM parameters for any diameter in the PC. This is demonstrated for two unfitted diameters in Fig. 6. It shows that the fitted functions indeed produce good compensation for diffusion in the detailed model. Therefore, we can use the fitted functions with morphologically detailed PC models.

Dendritic Ca^{2+} Spikes

Dendritic Ca^{2+} spikes with multiple spikelets comparable to those observed in vitro (Fig. 1b) were simulated using a single pool, a double pool, detailed Ca^{2+} dynamics, and DCM. Since the buffering models used in the simulations were different approximations of detailed Ca^{2+} dynamics, we expected the intracellular Ca^{2+} transients generated by these models to show considerable differences (Supplementary Fig. 3). Therefore, we first optimized values for the maximal conductance (G_{max} and P_{max}) of ion channels (current activation profiles are shown in Supplementary Fig. 4) in the model to generate as comparable Ca^{2+} spikes as possible. This is identical to the procedure that would be used to generate a neuron model with only one type of Ca^{2+} dynamics model [38]. The resulting values are listed in Table 2. The resultant voltage traces of the Ca^{2+} spikes are shown in Fig. 7 (see also Supplementary Fig. 2).

Comparing the dendritic Ca^{2+} spikes generated using different buffering models (Fig. 7a), we clearly see that the

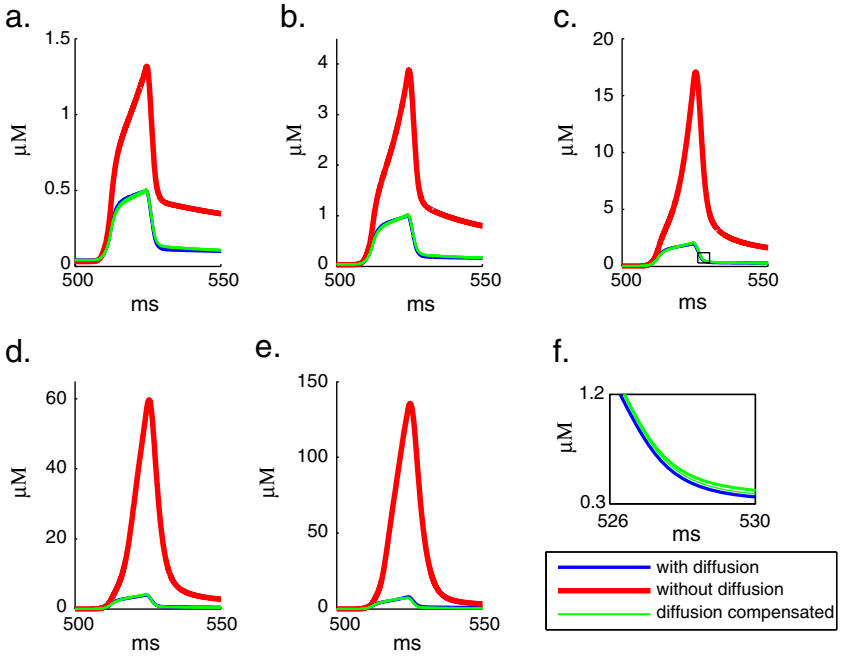

Fig. 4 Comparison of Ca^{2+} profiles of different peak amplitudes, **a** 0.5, **b** 1, **c** 2, **d** 4, and **e** 8 µM, simulated in a compartment with a diameter of 2 µm, using the detailed Ca^{2+} dynamics model, detailed Ca^{2+} dynamics model without diffusion, and DCM model. The removal of diffusion from the detailed model resulted in a steep rise in Ca^{2+}, which could be well compensated by DCM. The *inset* (**f**) below the panel (**c**) highlights Ca^{2+} profiles simulated using five different sets of optimal DCM parameters found by using Neurofitter

dendritic spikes generated using the pool-based models are different from the spikes generated using the other buffering models and strongly depend on the pool models used (compare Supplementary Fig. 2 with Fig. 7a). The amplitude as well as the width of second and third spikelets are different from the spikelets generated using the detailed Ca^{2+} model. Another noticeable difference exists in the after hyperpolarization of these bursts. These differences are due to the different activation of K_{Ca} channels, in particular of the SK channel (Supplementary Fig. 4). On the other hand, the dendritic Ca^{2+} spikes simulated using DCM approximated the Ca^{2+} spikes generated using the detailed Ca^{2+} dynamics model quite well.

A comparison of dendritic Ca^{2+} spikes over a time period of 50 ms may not reveal the effect of diffusion at longer time scales. Therefore, we ran all simulations for

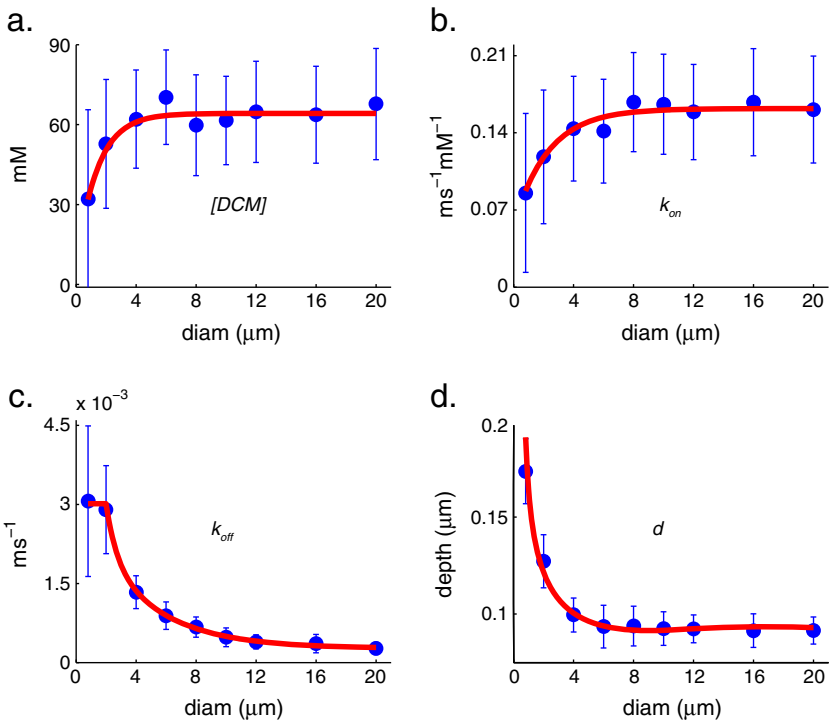

Fig. 5 Distribution of estimated DCM parameters ([DCM], k_{on}, k_{off}, and d; mean±STD, n=25: the five best solutions from five runs with different seeds for random number generation) for diffusion compensation plotted against compartment diameter. These were fitted respectively by **a** exponential function, **b** exponential function, **c** double exponential function, and **d** fifth order polynomial function

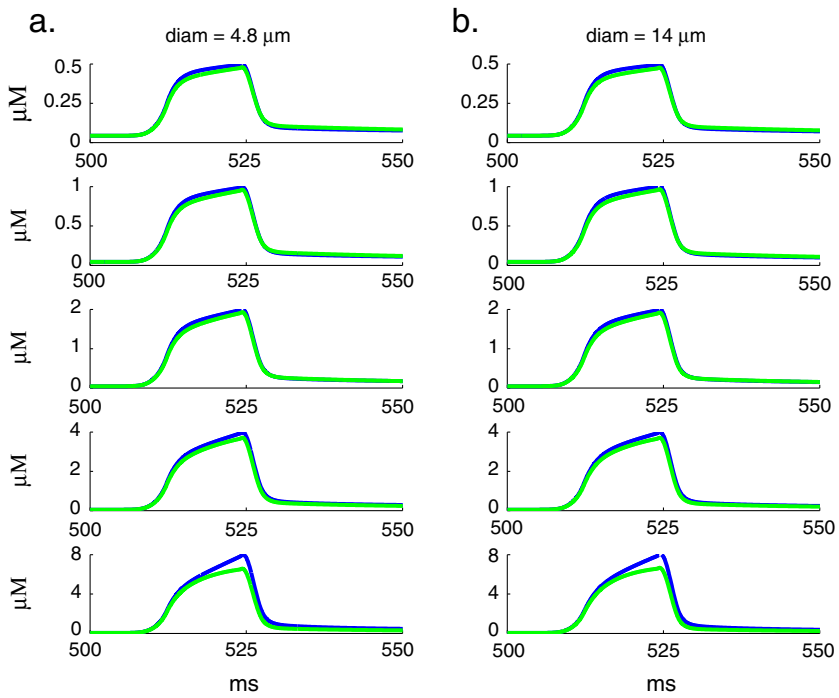

Fig. 6 Comparison of Ca^{2+} profiles of different peak amplitudes simulated using detailed Ca^{2+} dynamics (*blue*) and diffusion compensated Ca^{2+} dynamics (*green*) with predicted values of parameters for diffusion compensation mechanism from the functions in Fig. 5. **a** Diameter 4.8 µm. **b** Diameter 14 µm

200 s and compared the ability of different buffering mechanisms to capture the bursting behavior over that time. Fig. 7c, d shows the spontaneous dendritic Ca^{2+} bursting using the detailed Ca^{2+} dynamics model, DCM, single pool, and double pool models. Each of the bursts contains three Ca^{2+} spikelets (examples shown in Fig. 7a, b). The frequency of bursts in case of pool-based models is approximately five to six times higher than the frequency of bursts in the detailed Ca^{2+} dynamics model. However, the frequency of bursts for the DCM model is similar to that of the detailed model.

Comparing the burst of Ca^{2+} spikes around 57 s (marked with red asterisk in Fig. 7c, d) in Fig. 7b, we see that the shape has changed compared to the first burst (Fig. 7a), which is due to the buildup of Ca^{2+} over longer time. Pool-based models failed to capture this burst shape adaptation, while DCM reproduced it fairly well.

Next, we investigated the ability of DCM to approximate characteristics of diffusion over the longer time period when the bursting period was modified by current injection. The mean inter-burst interval plotted against the injected current is shown in Fig. 7e. The behavior of detailed Ca^{2+} dynamics model and DCM is similar at most current injection levels, except for bumps around 0.002 pA. These bumps represent the transition of the firing pattern from bursts with three spikelets to bursts with two spikelets (shown in Fig. 7f), which occurs at lower current levels in the detailed model. As the pool models do not show burst shape adaptation, they also entirely fail to capture this transition to two spikelet bursts. The spontaneous bursting period range is limited. Therefore, to compare the different buffering models at faster bursting rates, we injected current pulses at 1 Hz (Supplementary Fig. 5). Under these conditions, the Ca^{2+} buildup is more pronounced leading to a SK current mediated after hyperpolarization and a progressive decrease in the number of spikes in each burst, but the relative accuracy of the different buffering models is similar to that shown in Fig. 7.

Table 2 Maximal conductance values used to generate dendritic Ca^{2+} spikes

Buffering model	P_{max} (CaP) $\times 10^{-4}$ cm/s	P_{max} (CaT) $\times 10^{-6}$ cm/s	G_{max} (BK) $\times 10^{-2}$ S/cm^2	G_{max} (SK) $\times 10^{-4}$ S/cm^2
Single pool	1.87	7.32	5.34	6.07
Double pool	1.95	7.43	5.65	4.68
Detailed Ca^{2+} dynamics model	2.00	8.00	7.00	3.10
Diffusion compensated model	2.2	8.2	7.01	3.02

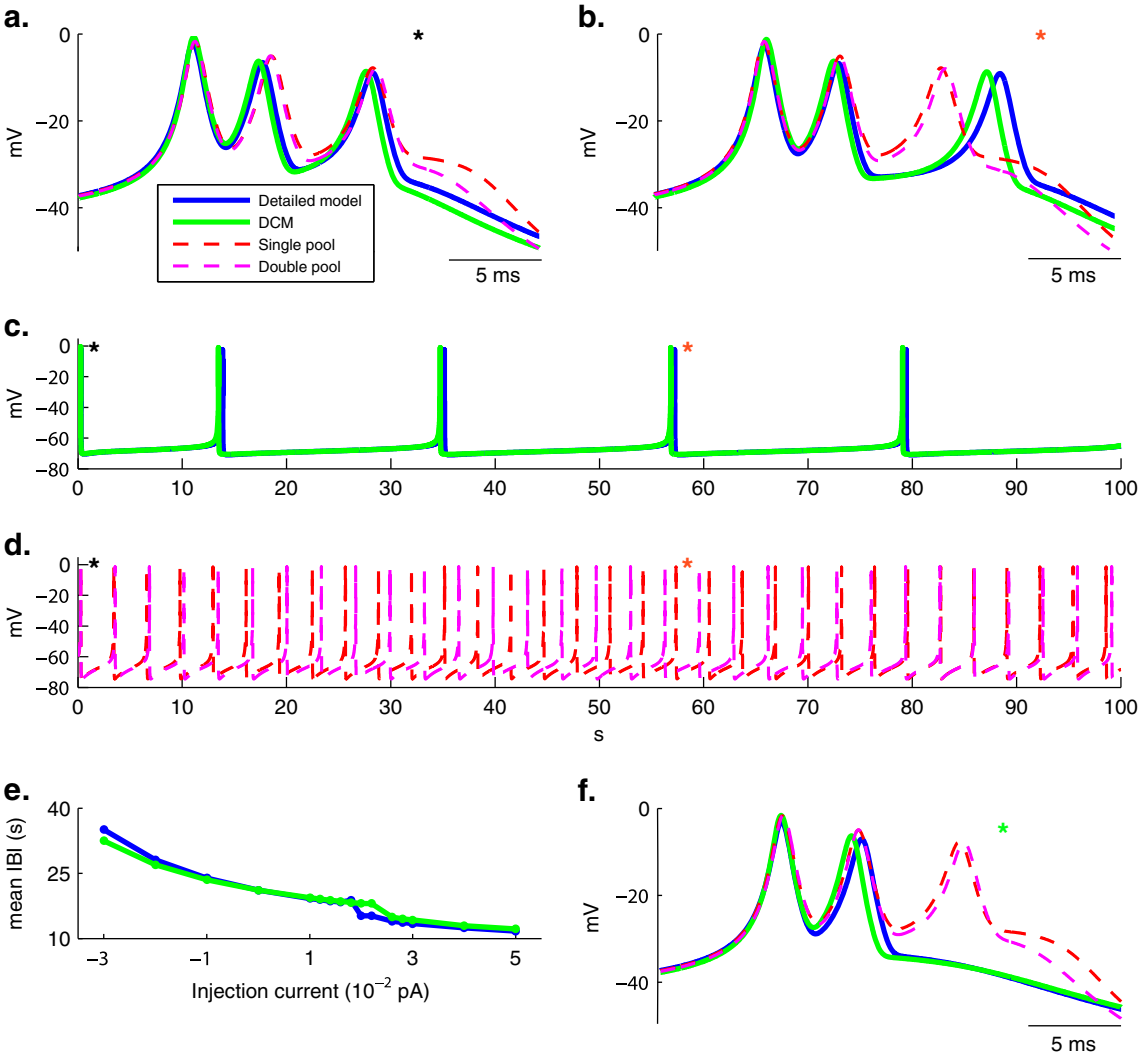

Fig. 7 Dendritic Ca^{2+} spikes generated using different Ca^{2+} buffering models (aligned at the peak of the first spikelet in **a**, **b**, and **f**). The parameters of pool-based models are those used in Supplementary Fig. 1. The conductance values used to generate these spikes are listed in Table 2. **a** First burst of Ca^{2+} spikes. **b** Burst of Ca^{2+} spikes around 57 s. **c**, **d** Spontaneous Ca^{2+} spike bursting over 100 s: *black asterisk* indicates the first burst of Ca^{2+} spikes (shown in **a**), *red asterisk* indicates the burst of Ca^{2+} spikes around 57 s (shown in **b**). **e** Inter-burst interval (IBI) as a function of current injection. **f** Burst of Ca^{2+} spikes around 57 s with injection of 0.004 pA current

Based on the data shown in Fig. 7, we conclude that DCM is quite effective over a wide range of conditions. While the approximation is not perfect, it is clearly much superior compared to the pool-based models. Finally, we briefly explored the robustness of DCM to changes in the Ca^{2+} buffers. Supplementary Fig. 6 shows a comparison of detailed and DCM models when the concentration of the CB and PV buffers is either halved or doubled (DCM parameters unchanged but ion channel densities retuned). The DCM approximation is very good for the half buffer concentration model, but less adequate for the double buffer concentration one. Therefore, we recommend to retune the DCM parameters whenever the detailed Ca^{2+} dynamics model is changed.

Discussion

We compared the effectiveness of different Ca^{2+} buffering mechanisms in controlling K_{Ca} channels expressed in PCs. The PC is known to express high amount of mobile endogenous buffers like calbindin and parvalbumin [39]. Ca^{2+} entering through voltage-gated channels is quickly removed by these buffers [19]. The internal Ca^{2+} stores and pumps together with calbindin and parvalbumin control the intracellular Ca^{2+} available to K_{Ca} channels. Therefore, careful modeling of intracellular Ca^{2+} dynamics is essential to simulate the physiological control of K_{Ca} channels.

The detailed Ca^{2+} dynamics model introduced by Schmidt et al. [25] includes calbindin, parvalbumin, pumps,

and diffusion of Ca^{2+}, parvalbumin, and calbindin. The model was tuned for Ca^{2+} dynamics in a single spine coupled to a dendrite. Since the spine is a small compartment, only longitudinal diffusion was modeled from the spine through the spine neck. In this study, we modeled dendrites, which are relatively large compartments; therefore, we modified the Schmidt et al. [25] model to incorporate radial diffusion towards the center of the compartment using the formalization implemented in NEURON [40]. Recent Ca^{2+} dynamics models [25, 41] used different pump rates to fit their data. We tuned the pump rate parameters to match the Ca^{2+} profiles recorded from a PC at high concentrations of Ca^{2+}, at which most of the buffers were saturated, and the decay could be attributed to diffusion and pump only [36].

The single Ca^{2+} pool has been the choice for modeling intracellular Ca^{2+} in almost all compartmental models. The volume of sub-compartment to compute the effective Ca^{2+} concentration for activation of K_{Ca} channels is often defined by a submembrane shell with a depth of 0.2 μm [20]. However, a wide range of decay rates (β values) is used from 10/ms [20] to 0.02/ms [42]. These parameter values used in single pool models can reasonably approximate the changes in microdomains [23] and can be used to control a BK-type K_{Ca} channel [17, 18]. SK-type K_{Ca} channels, which are relatively far from Ca^{2+} channels [18], require smaller amounts of Ca^{2+} (0–2 μM) and activate at relatively long time scales. Therefore, it is impossible to control both BK and SK channels correctly using a single pool. We confirmed this prediction by comparing the Ca^{2+} profiles (Supplemental Fig. 3) and dendritic Ca^{2+} spikes (Fig. 7 and Supplementary Figs. 2 and 5) generated by single pool and detailed models. We also considered a Ca^{2+} pool model with two time constants as a phenomenological solution to the problem. While such models fitted simple Ca^{2+} spikes better (Fig. 3), their concentration range is limited, and they fail to simulate the period of repetitive bursting and burst shape adaptation (Fig. 7).

The limitation of using detailed Ca^{2+} dynamics is the computational cost of underlying diffusion [27]. We computed run times for simulations of 10 s with detailed Ca^{2+} dynamics and different compartment diameters (Fig. 8). It took 45 s to run the simulation for a 2-μm diameter compartment. The run time increase was supra-linear with increase in diameter; for 20 μm, it was 1,076 s. This suggests that the computation cost will increase tremendously for simulating a morphologically detailed PC model, which we want to avoid. In this study, we proposed a method to approximate the effect of diffusion. Since only Ca^{2+} in the submembrane region is required to control K_{Ca} channels, it is not essential to compute the Ca^{2+} concentration in and around the center of compartments. We replaced diffusion with a compensating mechanism, DCM,

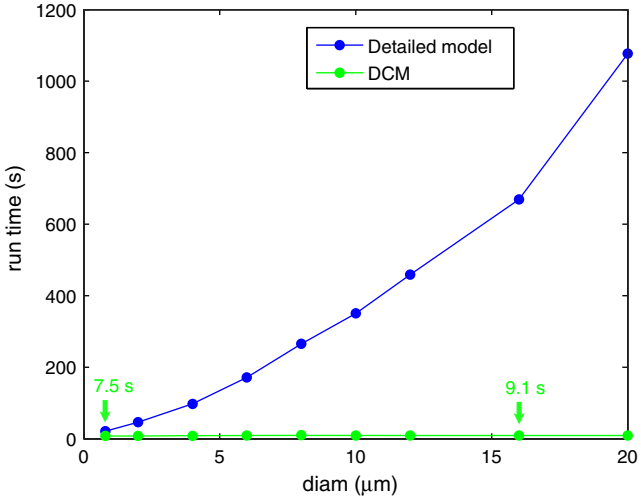

Fig. 8 Comparison of run time for NEURON simulations of 10 s, with detailed Ca^{2+} dynamics and with DCM using compartments with different diameters. All the simulations were run on an Apple MacBook Pro, Intel Core 2 Duo 2.33 GHz

that made up for the Ca^{2+} diffusing towards the center. We confirmed that the DCM approximated the effect of diffusion robustly in the range of 0.5–8 μM Ca^{2+} for dendritic compartments with diameters of 1–20 μm and over time ranges from tens of milliseconds to hundreds of seconds. Though BK channels are reported to sense approximately 100 μM of Ca^{2+}, those high concentrations are only available in nanodomains [18]. For volumes defined by ~0.1 μm shells, 8–10 μM of Ca^{2+} concentration should represent the limit of the physiological range [17]. To achieve this level of accuracy, it is important to fit the DCM parameters to the detailed Ca^{2+} dynamics model used (Figs. 4 and 5). For dendritic compartments with diameters less than 1 μm, the effect of diffusion is not significant and can be compensated by tuning only the depth (d) of the submembrane shell (results not shown in this work).

The method proposed in this paper is not limited to modeling PCs. The DCM parameters can be tuned to replace diffusion in large compartmental models of other neuronal types. To formulate robust DCM parameters, it is necessary to have a faithful detailed Ca^{2+} dynamics model of the specific neuronal type. Then, for the desired physiological range of Ca^{2+} influx and range of diameters in the morphology, DCM parameter equations can be derived to replace diffusion.

The use of the DCM resulted in a decrease of the run time to 8 s with a loss of dependence on diameter (Fig. 8). We conclude that using a detailed Ca^{2+} buffering model combined with DCM is a clear improvement compared to the Ca^{2+} pool for modeling Ca^{2+} dynamics in a large neuron model.

Acknowledgements We acknowledge Dr. Klaus M. Stiefel for providing the detailed Ca^{2+} dynamics model scripts which were extended for use in this work. This work was supported by OISTPC.

Conflicts of interest There is no conflict of interest in the work presented in this manuscript.

References

1. Gähwiler BH, Llano I. Sodium and potassium conductances in somatic membranes of rat Purkinje cells from organotypic cerebellar cultures. J Physiol. 1989;417:105–22.
2. Gruol DL. Chronic exposure to alcohol during development alters the membrane properties of cerebellar Purkinje neurons in culture. Brain Res. 1991;558(1):1–12.
3. Knaus HG, Schwarzer C, Koch RO, Eberhart A, Kaczorowski GJ, Glossmann H, et al. Distribution of high-conductance Ca(2+)-activated K+ channels in rat brain: targeting to axons and nerve terminals. J Neurosci. 1996;16(3):955–63.
4. Jacquin TD, Gruol DL. Ca2+ regulation of a large conductance K+ channel in cultured rat cerebellar Purkinje neurons. Eur J Neurosci. 1999;11(2):735–9.
5. Womack MD, Khodakhah K. Characterization of large conductance Ca^{2+}-activated K+ channels in cerebellar Purkinje neurons. Eur J Neurosci. 2002;16(7):1214–22.
6. Edgerton JR, Reinhart PH. Distinct contributions of small and large conductance Ca^{2+}-activated K+ channels to rat Purkinje neuron function. J Physiol. 2003;548(1):53–69.
7. Haghdoost-Yazdi H, Janahmadi M, Behzadi G. Iberiotoxin-sensitive large conductance Ca^{2+}-dependent K+ (BK) channels regulate the spike configuration in the burst firing of cerebellar Purkinje neurons. Brain Res. 2008;1212:1–8.
8. Cheron G, Sausbier M, Sausbier U, Neuhuber W, Ruth P, Dan B, et al. BK channels control cerebellar Purkinje and golgi cell rhythmicity in vivo. PLoS ONE. 2009;4(11):e7991.
9. Kaufmann WA, Ferraguti F, Fukazawa Y, Kasugai Y, Shigemoto R, Laake P, et al. Large-conductance calcium-activated potassium channels in Purkinje cell plasma membranes are clustered at sites of hypolemmal microdomains. J Comp Neurol. 2009;515(2):215–30.
10. Womack MD, Hoang C, Khodakhah K. Large conductance calcium-activated potassium channels affect both spontaneous firing and intracellular calcium concentration in cerebellar Purkinje neurons. Neuroscience. 2009;162(4):989–1000.
11. Stocker M, Pedarzani P. Differential distribution of three Ca(2+)-activated K(+) channel subunits, SK1, SK2, and SK3, in the adult rat central nervous system. Mol Cell Neurosci. 2000;15(5):476–93.
12. Cingolani LA, Gymnopoulos M, Boccaccio A, Stocker M, Pedarzani P. Developmental regulation of small-conductance Ca^{2+}-activated K+ channel expression and function in rat Purkinje neurons. J Neurosci. 2002;22(11):4456–67.
13. Womack MD, Khodakhah K. Somatic and dendritic small-conductance calcium-activated potassium channels regulate the output of cerebellar Purkinje neurons. J Neurosci. 2003;23(7):2600–7.
14. Yazdi HH, Janahmadi M, Behzadi G. The role of small-conductance Ca^{2+}-activated K+ channels in the modulation of 4-aminopyridine-induced burst firing in rat cerebellar Purkinje cells. Brain Res. 2007;1156:59–66.
15. Womack MD, Khodakhah K. Dendritic control of spontaneous bursting in cerebellar Purkinje cells. J Neurosci. 2004;24(14):3511–21.
16. Goldberg JA, Wilson CJ. Control of spontaneous firing patterns by the selective coupling of calcium currents to calcium-activated potassium currents in striatal cholinergic interneurons. J Neurosci. 2005;25(44):10230–8.
17. Zhuge R, Fogarty KE, Tuft RA, Walsh JV. Spontaneous transient outward currents arise from microdomains where BK channels are exposed to a mean Ca(2+) concentration on the order of 10 microm during a Ca(2+) spark. J Gen Physiol. 2002;120(1):15–27.
18. Fakler B, Adelman JP. Control of K(ca) channels by calcium nano/microdomains. Neuron. 2008;59(6):873–81.
19. Hartmann J, Konnerth A. Determinants of postsynaptic Ca^{2+} signaling in Purkinje neurons. Cell Calcium. 2005;37(5):459–66.
20. De Schutter E, Bower JM. An active membrane model of the cerebellar Purkinje cell. I. Simulation of current clamps in slice. J Neurophysiol. 1994;71(1):375–400.
21. Khaliq ZM, Gouwens NW, Raman IM. The contribution of resurgent sodium current to high-frequency firing in Purkinje neurons: an experimental and modeling study. J Neurosci. 2003;23(12):4899–912.
22. Akemann W, Knöpfel T. Interaction of Kv3 potassium channels and resurgent sodium current influences the rate of spontaneous firing of Purkinje neurons. J Neurosci. 2006;26(17):4602–12.
23. Sherman A, Keizer J, Rinzel J. Domain model for ca2(+)-inactivation of Ca^{2+} channels at low channel density. Biophys. 1990;58(4):985–95.
24. Tegnér J, Grillner S. Interactive effects of the gababergic modulation of calcium channels and calcium-dependent potassium channels in lamprey. J Neurophysiol. 1999;81(3):1318–29.
25. Schmidt H, Stiefel KM, Racay P, Schwaller B, Eilers J. Mutational analysis of dendritic Ca^{2+} kinetics in rodent Purkinje cells: role of parvalbumin and calbindin d28k. J Physiol. 2003;551(1):13–32.
26. Yamada WM, Koch C, Adams PR. Multiple channels and calcium dynamics. In: Methods in neuronal modeling: from ions to networks. Cambridge: MIT; 1998. p. 137–70.
27. De Schutter E. Modeling intracellular calcium dynamics. In: Computational modeling methods for neuroscientists. Cambridge: MIT; 2009. p. 93–106.
28. Hines ML, Carnevale NT. NEURON: a tool for neuroscientists. Neuroscientist. 2001;7(2):123–35.
29. Swensen AM, Bean BP. Robustness of burst firing in dissociated Purkinje neurons with acute or long-term reductions in sodium conductance. J Neurosci. 2005;25(14):3509–20.
30. Hille B. Selective permeability: independence. In: Ion channels and excitable membranes. Sunderland: Sinauer Associates; 2001. p. 441–70.
31. Iftinca M, McKay BE, Snutch TP, McRory JE, Turner RW, Zamponi GW. Temperature dependence of t-type calcium channel gating. Neuroscience. 2006;142(4):1031–42.
32. Cox DH, Cui J, Aldrich RW. Allosteric gating of a large conductance ca-activated K+ channel. J Gen Physiol. 1997;110(3):257–81.
33. Solinas S, Forti L, Cesana E, Mapelli J, De Schutter E, D'Angelo E. Computational reconstruction of pacemaking and intrinsic electroresponsiveness in cerebellar golgi cells. Front Cell Neurosci. 2007;1:2.

34. Hirschberg B, Maylie J, Adelman JP, Marrion NV. Gating of recombinant small-conductance ca-activated K+ channels by calcium. J Gen Physiol. 1998;111(4):565–81.
35. Sala F, Hernández-Cruz A. Calcium diffusion modeling in a spherical neuron. Relevance of buffering properties. Biophys J. 1990;57(2):313–24.
36. Maeda H, Ellis-Davies GC, Ito K, Miyashita Y, Kasai H. Supralinear Ca^{2+} signaling by cooperative and mobile Ca^{2+} buffering in Purkinje neurons. Neuron. 1999;24(4):989–1002.
37. Van Geit W, Achard P, De Schutter E. Neurofitter: a parameter tuning package for a wide range of electrophysiological neuron models. Front Neuroinformatics. 2007;1:1.
38. De Schutter E, van Geit W. Modeling complex neurons. In: Computational modeling methods for neuroscientists. Cambridge: MIT; 2009. p. 259–84.
39. Baimbridge KG, Celio MR, Rogers JH. Calcium-binding proteins in the nervous system. Trends Neurosci. 1992;15(8):303–8.
40. Carnevale NT, Hines M. How to expand NEURON s library of mechanisms. In: The neuron book. Cambridge: Cambridge University Press; 2006. p. 207–64.
41. Doi T, Kuroda S, Michikawa T, Kawato M. Inositol 1,4,5-trisphosphate-dependent Ca^{2+} threshold dynamics detect spike timing in cerebellar Purkinje cells. J Neurosci. 2005;25(4):950–61.
42. Traub RD, Llinas R. The spatial distribution of ionic conductances in normal and axotomized motorneurons. Neuroscience. 1977;2 (6):829–49.
43. Airaksinen MS, Eilers J, Garaschuk O, Thoenen H, Konnerth A, Meyer M. Ataxia and altered dendritic calcium signaling in mice carrying a targeted null mutation of the calbindin d28k gene. Proc Natl Acad Sci U S A. 1997;94(4):1488–93.
44. Allbritton NL, Meyer T, Stryer L. Range of messenger action of calcium ion and inositol 1,4,5-trisphosphate. Science. 1992;258:1812–5.
45. Nägerl UV, Novo D, Mody I, Vergara JL. Binding kinetics of calbindin-d (28 k) determined by flash photolysis of caged Ca(2+). Biophys J. 2000;79(6):3009–18.
46. Lee SH, Schwaller B, Neher E. Kinetics of Ca^{2+} binding to parvalbumin in bovine chromaffin cells: Implications for $[Ca^{2+}]$ transients of neuronal dendrites. J Physiol. 2000;525(2):419–32.

Model scripts All the scripts used to run simulations in this manuscript are available at ModelDB (http://senselab.med.yale.edu/ModelDB).